10 Measurement and Simulation Techniques

Our fundamental understanding of the boundary layer comes from measurements. Most measurements are made in the ***field***, some are made in ***laboratory tank*** or ***wind tunnel*** simulations, and some are samples from ***numerical simulations***. Theories and parameterizations, such as presented in earlier chapters, are valuable only if they describe the observed boundary layer behavior.

In this chapter we will outline the measurement categories, systems, field experiments, and techniques that are available to acquire a variety boundary layer data. Details of instrument design and operation will not be covered here, but they can be found in other references (see review by Lenschow, 1986).

10.1 Sensor and Measurement Categories

To make boundary layer measurements, we need three components: (1) a ***detector*** or ***sensor***, (2) an ***encoder*** or ***digitizer***, and (3) a ***data logger***. Most detectors are devices for which the physical characteristics (size, resistance, etc) change as a function of the variable being measured. Thus, virtually all detectors are ***analog*** in nature, providing a continuously varying output as a function of continuously varying meteorological conditions. This output signal must then be sampled to produce a discrete digital record, using some sort of encoder or ***analog-to-digital converter***. The resulting discrete series of data must be recorded, often on magnetic tape, magnetic disks, or optical disks. ***Instrument system*** or ***instrument package*** is the name given to the set of all three components listed above.

Additional components are also required: (4) an ***instrument platform***, (5) a means of ***calibration***, and (6) ***display devices***. Platforms such as a tower or aircraft are

complex and expensive in their own right, and can often hold or carry many instrument systems. Power supplies, cooling, sheltering or shielding, and accommodations for humans are sometimes part of the platform. Calibration against known standards either should be performed periodically during the measuring program, or should be accomplished continuously as an intrinsic function of the sensor or instrument package. Uncalibrated data is worthless data. Finally, the measured values should be displayed on printers, plotters, or video displays in order to confirm the operation of the instrument. Display can be real time showing the raw or digitized values, pseudo-real-time (within 5 to 30 minutes) showing summary tables and average statistics, or daily post-processing. It would be embarrassing to perform a long field experiment only to discover in the post experiment analysis phase that all the data is bad, missing, improperly recorded or uncalibrated.

Boundary layer data are split into two categories: those obtained from ***mean value*** sensors, and those from ***fast-response*** sensors. Fast-response sensors are used for measuring the turbulent fluctuations, from which we directly calculate turbulence kinetic energies, fluxes, and higher moments. These instruments are often complex, delicate and expensive. In the surface layer, turbulent eddies are relatively small and short lived, requiring sensors that have faster responses than ones used to measure eddies in the middle or top of the convective boundary layer. At nighttime, turbulence is sometimes weaker, requiring sensitive sensors that have a good ***signal-to-noise ratio***.

Fast-response instruments are also generally more costly to maintain, and require more expensive data logging equipment. The sensors are often small and delicate in order to achieve the fast response, and are thus vulnerable to damage by insects, precipitation, and mishandling. Either protective shrouds are needed, or replacements must be available. Since virtually all modern data logging is digital, the fast response signals are digitized at rates of once per second up to 50 or 100 times per second, resulting in data sets of thousands to hundreds of thousands of values for just a 20-minute record. The data logger must be able to ingest data at these high rates, and be able to store the large volume of data that accumulates.

If only mean values are required, then less-expensive, slower-response, more-durable instruments can be used. Based on profiles of mean variables, we can often indirectly calculate turbulence energies and fluxes. Most field experiments involve a mixture of mean and fast-response sensors, depending on the budget and the goals. Many of the fast-response sensors can also be used to find mean values, but not all.

Direct sensors are ones that are placed on some instrument platform to make ***in-situ*** measurements of the air at the location of the sensor. ***Remote sensors*** measure waves that are generated by, or modified by, the atmosphere at locations distant from the sensor. These waves propagate from the generation or modification point back to the sensor. ***Active remote sensors*** generate their own waves (sound, light, microwave), and have ***transmitter*** and ***receiver*** components. ***Passive remote sensors*** have only receiver components, and measure waves generated by the earth (infrared, microwave), the atmosphere (infrared), or the sun (visible).

Disadvantages of direct sensors include modification of the flow by the sensor or its platform, the fact that it gives a potentially unrepresentative point value, and the requirement to physically position the sensor in the part of the boundary layer where the measurement is to be made. Disadvantages of remote sensors include their size (large antennas or receiving dishes), cost and complexity, inability to measure certain boundary layer characteristics, their small signal to noise ratio which necessitates averaging over relatively large volumes (i.e., point values are not reliable), and the fact that the waves may be modified as they propagate back to the sensor. At present satellite-based remote sensors do not have adequate vertical resolution to provide much data in the boundary layer.

Advantages of direct sensors include sensitivity, accuracy, and simplicity. Advantages of remote sensors include the fact that they can quickly scan a large volume, area, or line of the atmosphere while remaining stationary on the ground, or located at convenient aircraft altitudes.

An additional trade-off between direct and remote sensors is the space/time required to acquire ***statistically stable turbulent moments*** (fluxes, variances). Lenschow and Stankov (1986) have shown that measurements by airborne direct sensors in convective boundary layers theoretically must be made over distances of about 10 to 100 km for turbulent variances, about 100-10,000 km for scalar fluxes, and 1000 to 100,000 km for stress, in order to achieve 10% accuracy. In many cases, it is impossible for flight legs of the required distance to be flown. Measurements over shorter distances would yield statistically nonrobust data that has a lot of scatter, such as demonstrated by the fluxes plotted in Figs 3.1 - 3.3 that were computed from data over 20 km flight legs. Remote sensors, which can scan large volumes in short times, can potentially achieve a much better statistical average, and are becoming more popular.

10.2 Sensor Lists

The large variety of sensors that have been developed is staggering. In the lists below, sensors that have been frequently used for fast-response measurements are flagged with (*). After each sensor is a brief explanation of the physical properties involved.

10.2.1 Temperature - thermometers

Direct Sensors:
liquid (mercury or alcohol) in glass - liquid expands higher into glass tube
wax thermostat - wax expands; e.g., automobile thermostats
bimetallic strip - two metals expand at different rates, causing bimetallic strip to bend
thermocouple * - junctions between different wires (copper & constantan) generate voltage
thermistor * - semiconductor electrical characteristics change
resistance wires/hot wires * - electrical resistance changes
sonic anemometer/thermometer * - speed of sound varies
melting/freezing points for different chemicals - e.g., wax melts on paper, changing color
quartz crystals - electronic resonance frequency changes

liquid crystals - optical characteristics, like color or darkness, change
crickets - chirp rates change
chemicals - reaction rates change

Remote Sensors:
microwave sounders - microwave propagation/ refractive index
DIAL lidar - dual wavelength laser radar
mirages - refraction of visible images
scintillation * - refraction of laser light beam in regions of temperature variation
radiometers * - emitted (black body) radiation
sodar * - scattering of sound off of regions of temperature variation

10.2.2 Humidity - hygrometers

Direct Sensors:
psychrometers - water evaporates from wick over thermometer, causing cooling
hair hygrometer - absorption of water causes organic fiber to expand
chilled mirror (dew pointer) - surface cooled to cause condensation
hygristor - electrical resistance of a chemical on a glass plate changes with humidity
Lyman-alpha and IR hygrometers * - absorption of radiation by water vapor
microwave refractometer * - index of refractivity changes
nephelometer - visibility changes
chemical reactions and alterations in biological life forms

Remote Sensors:
lidar - aerosol swelling in humid air
radar - variations in refractive index

10.2.3 Wind: Velocity - anemometers
Direction-vanes

Direct Sensors:
cup - drag against cups causes rotation on axis perpendicular to wind
propeller - turns blades on axis parallel with wind
Gill * - this is a lightweight variety of propeller anemometer
hot wire *- electrical current needed to maintain temp. of wire against cooling of wind
sonic * - speed of sound
pitot/static * - dynamic pressure increase associated with deceleration of wind into orifice
aspirator - pressure decrease associated with air flow across an orifice
drag sphere - drag force experienced by sphere, measured by strain gauges
pivot arm - hanging rod or plate that is blown against gravity or spring
gust vane * - measures v' or w' via lateral forces on vane (strain gauges or movement)
pibal - pilot balloon tracked by theodolite or radar
venturi - pressure drop related to Bernoulli effect

rotometer - fluid moving vertically in conical tube lifts a ball in tube
Beaufort scale - wave height or sea state
Fujita scale - damage assessment
wind vane - points in horizontal compass direction wind comes from
bivane - pivots up/down as well as left-right to give elevation angle and compass direction

Remote Sensors:
Doppler radar - Doppler frequency shift parallel to beam of microwaves
Doppler sodar - Doppler frequency shift parallel to path of sound
Doppler lidar - Doppler frequency shift parallel to laser beam
lidar - manual/statistical (autocorrelation) tracking of aerosol structures, any angle to beams

10.2.4 Pressure - barometers & microbarographs

Direct Sensors:
aneroid elements * - compression of evacuated container against restoring force of spring
capacitive elements * - capacitance of sealed volume changes as container walls move
mercury in glass - weight of mercury balances pressure

Remote Sensors:
None that use wave propagation directly, but some that measure temperature and velocity fluctuations as mentioned above, and infer pressure perturbations as residual from governing equations.

10.2.5 Radiation - radiometers

Most radiometers measure the radiative warming of a tinted surface, where the surface is protected from conductive and convective heating inside a glass or plastic hemispherical or spherical chamber. Depending on the type of tinted surface and the exposure, the radiometer can be designed to measure radiation in specific frequency bands coming from specific directions:

radiometer - total radiation (all wavelengths) from all directions within one hemisphere (upward or downward) hitting a plane surface that is parallel to local horizontal
net radiometer - difference between top and bottom hemispheres
pyranometer - short wave (solar) radiation, one hemisphere, plane horizontal surface
net pyranometer - difference between top and bottom hemispheres, short wave only
pyrheliometer - short wave direct beam radiation normal to surface (shielded from diffuse)
diffusometer - pyranometer with a device to shade it from direct sunlight
prygeometer - long wave (IR), one hemisphere, plane horizontal surface.

10.3 Active Remote Sensor Observations of Morphology

Radars (radio detection and ranging) transmit microwaves, ***sodars*** sound, and ***lidars*** light. Some use pulsed transmissions, while some are continuous. By measuring the time from when a pulse was transmitted until a signal is returned, the distance to the feature that returned the signal can be calculated. If pulses or ***shots*** are aimed in different directions, then the resulting signals can be constructed into ***scans***. By measuring the frequency (Doppler) shift in the signal, radial velocities can be found.

Active remote sensors can scan planes or volumes in the atmosphere, allowing us to compose "snapshot" like pictures of the boundary layer. With this capability we can examine the shape and form of turbulent eddies and convective elements (i.e., the ***morphology*** of turbulence structures). By ***looping*** through a series of successive snapshots in the cinematographic sense, we can watch the evolution of these elements. Noonkester (1979) has suggested a way for cataloging the different types of structures visible using remote sensors.

For stationary sensors on the ground, vertical scans at a fixed azimuth angle give what is called an ***RHI (range-height indicator)*** display. This is essentially a vertical cross section of the boundary layer. Scans through a range of azimuth angles, but with the elevation angle fixed, gives the ***PPI (plan-position indicator)*** display. For very low elevation angles, the PPI display is almost the same as a horizontal cross section. Modern data analysis algorithms allow volume scans to be remapped into horizontal or vertical cross sections.

Pseudo-RHI scans are made by fixed sensors looking only vertically. As the wind blows boundary layer structures over the sensor, the resulting sequence of shots with time can be interpreted as a vertical cross section by employing Taylor's hypothesis. True vertical cross sections are obtained from downward or upward-looking sensors mounted on aircraft.

In the absence of precipitation or chaff particles, radar and sodar detect variations in the refractive index of the air that are on the same order as the wavelength of the sensor. For radar, these fluctuations are most strongly related to moisture fluctuations of centimeter scales, while for sodar they are related to temperature fluctuations of meter scales. If there are regions in the boundary layer where such moisture or temperature variations exist, whether as active turbulence or as footprints of former turbulence, then some of the wave energy transmitted from the remote sensor will be scattered off of this region back to the sensor. So little energy is scattered back to the detector that very powerful pulses of energy must be transmitted, and very sensitive receivers must be designed to measure the returns. In the simplest displays, the regions of higher-intensity returned signals are plotted as a bright spots, relative to the dark areas of little returned signal.

10.3.1 Radar

Sketches of returned signal for radar RHI returns are shown in Fig 10.1a. In fair weather conditions, the boundary layer is often more humid than the free atmosphere. Thus, centimeter-scale eddies on the interface between the mixed layer and the free atmosphere create strong returns. Within the mixed layer there is little returned energy in spite of the strong turbulence, because the humidity is high everywhere. Similarly, there is usually little returned energy in the free atmosphere, because the humidity is low everywhere. Sometimes, however, layers of moist air aloft allow clear air turbulence regions to be visible on radar, exhibiting a characteristic "cats eye" pattern.

Normal weather radar is neither powerful nor sensitive enough to detect most clear-air boundary layer phenomena; so only a smaller number of research radars have been used for this work. These research radars can detect turbulence from near the surface up to the top of the troposphere. A variety of ground-based automated microwave ***atmospheric sounders*** have also been developed for deployment and operational gathering of wind and other meteorological data.

Fig 5.8 shows the difference between mechanical turbulence (forced convection) and convective turbulence (free convection) as viewed by radar. Free convection exhibits the characteristic upside-down "U" shaped returns associated with the tops of thermals. Mechanical turbulence creates a more random and torn return, with tilts in the displayed structures giving evidence of wind shear. Radar returns for stable boundary layers are plotted in Fig 10.1d. Fig 10.1g shows PPI scans of free convection, where the horizontal slices through thermals show circular or "donut"-like patterns around the perimeter of the thermals.

Even in cloud-free boundary layers, there may be enough insects to enhance the scattering back to the radar. In some field experiments, chaff is dispersed to create even more returns. Chaff are fine hair-like strands of plastic, coated with a thin layer of aluminum or other conductor. These strands are cut to the wavelength (or fraction or multiple of the wavelength) of the microwaves, and are dispensed in the air either from aircraft or from the ground. Their light weight causes their terminal velocity to be almost zero, and allows them to be carried aloft and dispersed by the turbulence.

10.3.2 Sodar

Sodars (sometimes called ***acoustic sounders***) send an audible "beep" of sound, generated by powerful loudspeaker horns. The returned sound is usually focused by a parabolic dish into a sensitive microphone, which serves as the detector. To reduce the amount of ambient background noise entering the system, shelters and acoustic screens are usually erected around the dish/microphone receiver, or else the receiver is placed in a hole below ground. Otherwise, noise from rustling leaves, wind noise, traffic, and conversation can contaminate the desired signal.

Sodar detects the interface at top of the mixed layer, using variations between the cooler mixed layer air and the warmer temperature inversion air capping the mixed layer.

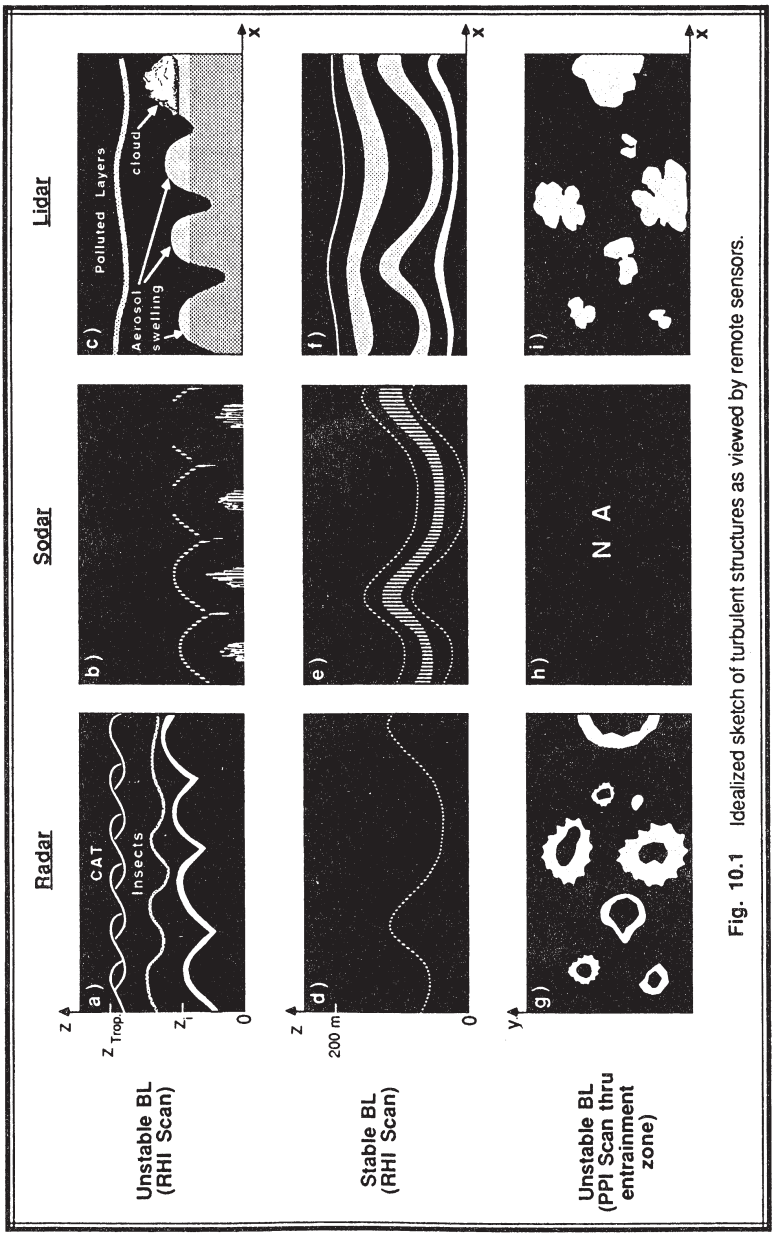

Fig. 10.1 Idealized sketch of turbulent structures as viewed by remote sensors.

Unfortunately, sound is attenuated so rapidly in the atmosphere that it is difficult to detect structures beyond a range of about 1 km. Since many mixed layers grow to heights above 1 km in the afternoons, the sodar is useless for determining z_i except in the early morning. Sodars can see the roots of thermals in the surface layer (see Fig 10.1b). Sodar is particularly valuable at night, where it detects buoyancy waves and turbulence in the stable boundary layer (Fig 10.1e).

10.3.3 Lidar

Lidars transmit laser light, which is scattered off of air molecules, cloud droplets and aerosols in the boundary layer. The returned light is collected in a telescope and focused on a photomultiplier detector, after which it is amplified, digitized and recorded. Because the source of many aerosols is the earth's surface, the boundary layer often has a higher concentration than the free atmosphere. As a result, the whole boundary layer often provides strong lidar returns, which stands out in the display as a deep white area, compared to the darker free atmosphere. Thus, the lidar sees the boundary layer air, rather than just the interface at the top of the boundary layer.

Fig 10.1c shows sketches of RHI lidar returns for a convective mixed layer, where individual thermals are often visible within the polluted mixed layer. Sometimes elevated haze layers are also visible. Aerosol swelling in the high relative humidities at the top of the mixed layer cause enhanced lidar returns, which show up brighter on the display. Clouds have such strong reflection and absorption that a strong return is generated at the base or the side of the cloud illuminated by the light. After a few tens of meters into the cloud, the light is so attenuated that there are nor more returns. Thus, the cloud appears opaque, and leaves a shadow behind it. Pollutants are also easily tracked by lidar.

In statically stable conditions, there is frequently a change of wind direction with height within the lowest few hundred meters of the ground. As a result, air from different source regions with different aerosol contents are advected into the region. This frequently causes a layer-cake appearance, with thin horizontal strata of different brightness on the RHI display (Fig 10.1f). When buoyancy waves exist, the strata also look wavy.

Lidar PPI displays of convective mixed layers (Fig 10.1i) show irregular perimeters to the thermals. Time lapse loops indicate lateral entrainment, or ***intromission***, into the thermals analogous to the vertical entrainment at the top of the whole mixed layer. Near the center of the thermals there are sometimes undiluted cores.

10.4 Instrument Platforms

Fig 10.2 shows a sketch of the instrument platforms to be described below. These platforms provide the physical/structural support for the sensor, shielding for the sensor, electrical power, and sometimes chemicals necessary for the measurements.

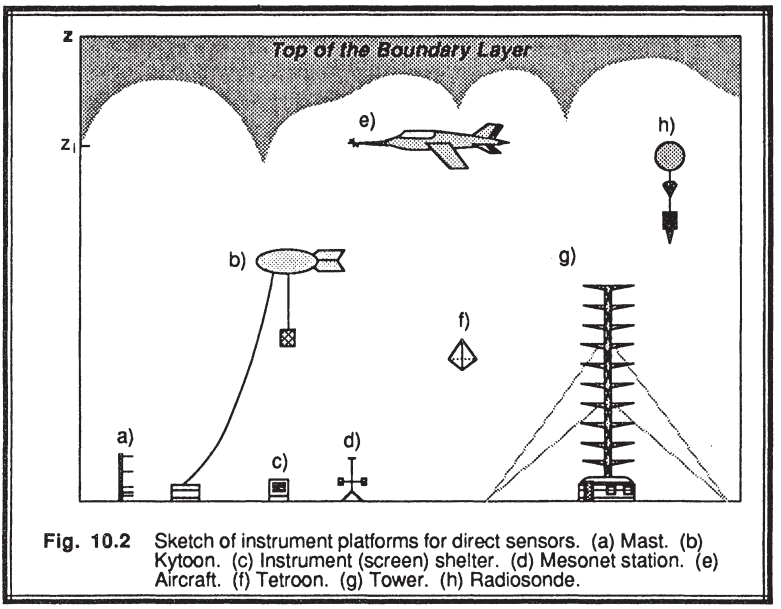

Fig. 10.2 Sketch of instrument platforms for direct sensors. (a) Mast. (b) Kytoon. (c) Instrument (screen) shelter. (d) Mesonet station. (e) Aircraft. (f) Tetroon. (g) Tower. (h) Radiosonde.

10.4.1 Instrument Shelters

The classical white louvered instrument shelter, called the ***Stevenson screen***, is mounted on a stand to place the instruments inside at a height of about 2 m above the local ground level. The shelter protects the instruments from the sun, but it also filters out much of the smaller scale turbulence. As a result, we can expect to measure mean quantities such as temperature, humidity, and pressure within the shelter. Otherwise, this platform is not used very often for micrometeorological measurements.

10.4.2 Masts

A mast is a pole upon which instruments can be placed at a variety of heights. Sometimes scaffolding is used to erect a short tower. A typical mast height is 10 m to 50 m. It is relatively inexpensive, and can be erected with simple equipment. Because of its limited height, it is primarily useful for surface layer measurements. Sensors are often placed closer together at the bottom of the mast than at the top, because profiles of temperature, wind, and humidity vary approximately logarithmically with height. For example, at the Minnesota experiment (see Table 10-1), temperature sensors were placed at z = 0.5, 1, 2, 4, 8, 16, and 32 m. Such masts can be easily transported and erected for a field program, and then dismantled when the experiment ends. Wires carry the signals down the mast to a data logger or data trailer close by.

10.4.3 Portable Mesonet Stations

A variety of quasi-portable surface stations exist that can be deployed for field experiments. A typical implementation will consist of temperature, humidity, rain, pressure, and radiation measurements at $z = 2$ m, and a 10 m mast to measure wind speed and direction. Some stations have additional sensors to measure turbulent fluxes directly, while others make measurements of mean variables at two or more heights to infer fluxes (see Section 10.7). Data is transmitted to a central recording site via satellite, radio, or telephone lines.

10.4.4 Towers

Tall expensive towers have been erected at a few sites for permanent use. Examples include the 213 m tower near Cabauw, about 50 km southeast of the North Sea coastline in The Netherlands. Another is the 300 m Boulder Atmospheric Observatory (BAO) tower in Colorado, about 25 km east of the Rocky Mountains. Occasionally, existing television transmitting towers are instrumented, such as the 444 m KYTV tower in Oklahoma City. Towers are useful for studying the nighttime and early morning boundary layers that are shallow.

These are large structures with built-in elevators and many support guy wires. Because the tower is so large, it disturbs the flow close to it and downwind of it. For this reason, these towers have large horizontal booms that project horizontally away from the tower at different heights, upon which sensors are mounted. At each height, there are often booms projecting in 2 or 3 different compass directions, with the expectation that at least one of the booms will be in the upwind direction. Permanent buildings housing the communications, data logging, maintenance, and computer facilities are sometimes built near the tower.

10.4.5 Kytoons

A kytoon is an aerodynamically shaped helium-filled plastic balloon that is tethered to a winch on the ground. Instead of being blown down by the wind, the shape allows it to soar upward like a kite — hence the name kytoon. In typical applications, a sensor package is suspended a short distance below the balloon on lines different from the tether line. To make measurements at a variety of heights, the winch is used to draw in or feed out more line until the desired height is reached. The balloon is kept at each height of interest for 5 to 30 minutes to get a statistically stable sample, before changing its altitude. Also, the balloon can make measurements while it is rising or descending, allowing soundings to be recorded. In some cases, the instrument package sends its signals down electrical wires attached to the tether cable, while for other kytoons a transmitter radios the information to the ground. Although tethers on the order of 1.5 to 2 km are available, flight regulations sometimes restrict deployment to altitudes below about 800 m. Kytoons are much more portable than tall towers, and can easily be used at temporary field experiments, but they are limited to light winds.

Occasionally, tethered balloons are flown with instruments deployed at a variety of heights along the tether cable. Although these offer the advantage of simultaneous measurements at a number of heights, they are more difficult to deploy and pull back in.

10.4.6 Free balloons

A ***radiosonde*** is an expendable instrument and transmitter package attached below a free-flying helium balloon that measures temperature, humidity, and pressure. ***Rawinsondes*** also provide wind information, either by a tracking antenna on the ground, or via LORAN or OMEGA receiving systems in the instrument package itself. Observations from radiosondes or rawinsondes are called ***raobs***. Special balloons and instrument packages are designed for boundary layer experiments, where the balloon rises more slowly, and the instrument package makes measurements at more heights within the boundary layer. Although each balloon package is not too expensive, the cost during a field program can be surprisingly expensive if balloons are launched frequently. For boundary layer work, the raob is difficult to utilize because it is often an unrepresentative point measurement that provides neither a time nor a space average. These balloons drift away from the launch site and rise until they burst, allowing the instrument package to parachute to the ground.

10.4.7 Tetroons

A special class of free balloon is the constant pressure balloon. Instead of being made of latex like radiosonde balloons, these are made of an unstretchable material such as mylar plastic. These balloons are often constructed in the shape of a tetrahedron — hence the name tetroon. When inflated and properly balanced, the balloon will rise to an altitude where the air density matches the balloon system overall density, allowing the balloon to theoretically stay at a constant (pressure) altitude. In reality, the balloon will often make large amplitude vertical oscillations about its mean altitude. Sometimes instrument systems are suspended from the balloon, while for other experiments a radar reflector or transmitter is suspended, to allow the balloon to be tracked for tracer dispersion studies.

10.4.8 Aircraft

A variety of aircraft ranging from model drones, ultralights, gliders, motorgliders, light single and multiengine propeller aircraft, multiengine turboprop, multiengine jet, and cabin-class civilian and military transports have been used as platforms for boundary layer study. Typically, instruments are mounted on special booms projecting forward from the nose or the wings of the aircraft, in order to get the sensors out of the flow disturbed by the aircraft itself. Some sensors are built into the radome, while others use remote sensing techniques to detect the flow in front of the aircraft. The larger aircraft allow on-board computer equipment to process the data, and airborne scientists can view real-time displays to help direct the experiment. Turbulence sensors must have a very fast

response, because typical aircraft speeds are 50 to 100 m/s.

Typical boundary layer flight patterns consist of level horizontal flight legs of 10 to 20 minute duration in order to get a large enough sample to generate stable turbulence statistics. These legs are flown either over fixed tracks on the ground, or are flown in "L" patterns with one leg parallel to the current wind direction and the other leg in the cross-wind direction. In addition to legs flown at a variety of heights in the boundary layer, some ascent or descent soundings are made that yield much more representative vertical profiles than raob soundings.

As described in section 10.1, it might be impossible to fly a pattern of the proper length to gather data with robust statistics. Flight legs that are too short have potentially large sampling errors, yielding large scatter in the data. Flight legs that are long enough for stable statistics can consume so much flight time that stationarity within the BL might be violated. The way around this problem is to fly a faster aircraft, but the airborne sensors must have a correspondingly faster response, which might be difficult or impossible.

10.4.9 Platforms for remote sensors

As of the writing of this text, most remote sensing systems were so large that they were limited to either the larger aircraft, or to fixed or mobile surface sites.

10.5 Field Experiments

Because fast-response turbulence data is not routinely collected by most operational weather services, it is necessary to conduct special field programs. Some of the early experiments focused on surface layer data over flat uniform terrain or oceans. Later experiments probed higher in the boundary layer and/or picked a nonuniform site or shorelines. Table 10-1 summarizes the major experiments that were either completely devoted to boundary layer measurements, or had a major boundary layer subprogram.

Many of these experiments have resulted in the publication of data books, which are available from the lead principal investigator, the sponsor, or government printing offices. These field experiment names appear frequently in the literature, because they provide the data set against which theories and models are tested.

Table 10-1. Chronological summary of field programs that gathered boundary layer data. Abbreviations used for data collected: A=aircraft, B=raobs, C=chemistry, D=dispersion, E=surface energy budget, F=turbulent fluxes, G=(below) ground & soil data, g=geostrophic, H=hydrologic & precipitation, K=radiation, K2=kytoons, L=lidar, O=ocean, P=pressure, p=vertical profile, R=radar, S=sodar, s=surface, T=temperature, TKE=turbulence, U=uniform land, V=wind, WX=weather & clouds. (* = incomplete information)

Short Name	Date	Location	Data Book or Reference, Long Name, Data Gathered
Great Plains	Aug-Sep 53	O'Neill, Nebraska, USA	Lettau & Davidson (1957). All except R,S,L,O.
Wangara	Jul-Aug 67	Hay, Australia	Clarke et al (1971). All except TKE,H,F,D,C,L,R,S,A,O
Kansas	Jul-Aug 68	SW Kansas, USA	Izumi (1971). 32m mast - surface layer data: F,TKE,U, Tp,Vp.
BOMEX	May-Jul 69	Barbados, Caribbean	Kuettner & Holland (1969). BOMEX=Barbados Oceanog. & Meteor. Exp. All except U,S,L,C,D
Marsta	69-71	Marsta, Sweden	Smedman-Högström ... (1973), Högström 1974), (DeHeer-Amissah (1981). All but H,D,C,A,K2,L,R,S,O
METROMEX	Summers 71-76	St.Louis, Missouri, USA	Changnon (1981). METROMEX = Metropolitan Meteor. Exp. All except O,U,L
VIHMEX	May-Sep 72	Carrizal, Venezuela	Betts & Miller (1975). VIMHEX=Venezuelan Internatl. Meteor. & Hydrolog. Exp. R,B,Ts,WX,Vs
Minnesota	Sep 73	NW Minnesota, USA	Izumi & Caughey (1976). 32m mast-sfc layer:F,TKE,U, Tp,Vp,K2.
Cabauw/C	1973-1984 (Continuous)	Cabauw tower, The Netherlands	Monna and Van der Vliet (1987), Wessels (1984). All except TKE, F, D, A, K2, L, R, O
Koorin	Jul-Aug 74	Daly Waters, Australia	Clarke & Brook (1979). All except TKE,H,D,C,L,R,S,O
GATE	Summer 74	Tropical Atlantic & W.Africa	Multinational, organized by WMO. Kuettner & Parker (1976); GATE=GARP Atlantic Tropical Exp., GARP = Global Atmos. Res. Prog. All but U, L, D, G.
AMTEX	Feb 74, 75	East China Sea, off Japan	Lenschow & Agee (1976). AMTEX=Air Mass Transformation Exp. All except G,D,C,K2,L,S,U
BLS77	May-Jun 77	Chickasha, Olkahoma, USA	Hildebrand (1980). BLS77=Bound. Layer Structure 1977. T,V,P,p,s,TKE,K,WX,F,R
VOVES	Jul 77	Voves-Villeau, Central France	André & Lacarrere (1980). All except H,D,C,K,L,O
Cabauw/E	1977-1979	Cabauw tower, The Netherlands	Monna and Van der Vliet (1987), Nieuwstadt (1984). All except D, A, K2, L, R, O
PHOENIX	Sep 78	At BAO tower Boulder, Colorado, USA	Hooke (1979). All except H,D,C,U,O
SESAME	Apr-Jun 79	Oklahoma, USA	AMS SESAME News (1979-82): SESAME=Severe Environ. Storms & Mesoscale Exp. All except O,S,L,D

CCOPE	May-Aug 81	Miles City, Montana, USA	Knight (1982). CCOPE=Cooperative Convective Precip. Exp. All except O,S,L,K2,C,D,G
PUKK/ KONTUR	Sep-Oct 81	German Bight, North Sea coast	Hoeber(1982), Kraus(1982), Kontur(1985).KONTUR =convect. &turb. over sea. All except F,C,K,L,R,D,G,H
COAST	May 83	Dutch coast	Weill, et.al. (1985), Desbraux & Weill (1986). Coastal meteor. All except D,C,K,L,R
BLX83	May-Jun 83	Chickasha, Oklahoma, USA	Stull & Eloranta (1984), Stull et.al. (1988). BLX83=Bound. Layer Exp. 1983. All except H,D,O
Øresund	Summer 84	Denmark & Sweden	Gryning (1985, 1986). Mesoscale dispersion land-water-land. All except C,K,L
PHOENIX II	May-Jul 84	At BAO, Colorado, USA	Lilly(1984). BL evolution. All except G,g,H,D,C,K,L,S,U,O
MESO-GERS	Sep-Oct 84	SW France	Weill, et.al. (1987). Mesoscale. All except G,D,C,K,L,O
PRE-STORM	May-Jun 85	Oklahoma & Kansas, USA	Cunning, J.B. (1986). PRE=Preliminary Regional Exp. of STORM-Central. All except G,D,C,K,L,S,O
ABLE	Jul-Aug 85 Apr-May 87	Manaus, Brazil	Harris (1987), also J. Geophy. Res. ABLE=Amazon . Boundary Layer Exp. All except D,S,O
DYCOMS	Jul-Aug 85	East Pacific off California, USA	DYCOMS=Dynamics and Chemistry of Marine Stratocumulus. All except s,G,g,H,K,D,L,R,S,U,E*
GALE	Jan-Mar 86	New England USA & Atlantic	AMS (1985). GALE=Genesis of Atlantic Low Exp. All except U,D,G
FASINEX	Feb-Mar 86	Atlantic near Bermuda	Stage & Weller (1985,86). FASINEX=Frontal Air Sea Interaction Exp. All except U,C,D,G
HAPEX	May-Jul 86	SW France	André, et.al. (1986, 1988). HAPEX = Hydrologic-Atmos. Pilot Exp. All except O,D,L,C
HEXOS	Autumn 86	North Sea, The Netherlands	Katsaros, et.al. (1987). HEXOS=Humidity EXchange Over the Sea. All except G,K,U,C,D.
TAMEX	May-Jun 87	Taiwan	TAMEX=Taiwan Area Mesoscale Exp.*
FIFE	May-Nov 87	Manhattan, Kansas, USA	FIFE=First ISLSCP Field Exp., ISLSCP=Internatl. Satellite Land Surface Climatology Proj.*

10.6 Simulation Methods

Although field measurements represent "truth" by definition, it is a truth that is composed of the superposition of many simultaneous effects and processes. For a few situations, we can attempt to isolate or focus on one specific process by the careful selection of a field site (e.g., uniform terrain) or weather pattern (e.g., fair weather). However, we can never fully isolate any one process, and the weather is rarely reproducible. Also, it is difficult to do sensitivity studies by systematically altering certain physical parameters, and then measuring the effects.

We can partially circumvent these difficulties by creating an artificial turbulent domain where only a limited number of processes or boundary conditions acts on the flow. Such simulations can be created physically in laboratory tanks and wind tunnels, or numerically via computer models. In both cases, we must (1) create a model of the real atmospheric situation, (2) run the model to generate the turbulence; (3) sample the turbulent field much the same way the the real atmosphere is sampled; and (4) compute turbulence statistics (fluxes and means) from the sampled field. If sufficient care is taken to create a realistic model, then we can often learn more, faster, and with less expense than by conducting a field program.

10.6.1 Numerical

In Chapters 2-5 the equations of motion were Reynolds averaged to statistically separate the mean flow from the turbulent perturbations. Instead of taking that route, suppose we use the raw equations of motion to forecast velocities and temperatures at every point in a (hypothetical) modeled turbulent domain; then we should be able to forecast turbulent motions ***deterministically***. For example, in certain regions we might see warm updrafts simulating convective thermals, other points simulating wave motions, and yet others exhibiting apparently random variations characteristic of isotropic turbulence.

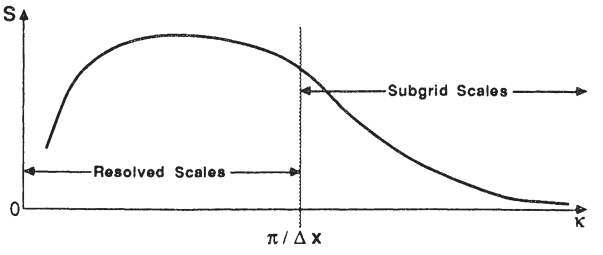

Fig. 10.3 Eddies larger (wave numbers smaller) than $2\Delta x$ are explicitly resolved by the model, while smaller eddies are subgrid scale and must be parameterized. If the grid spacing is such that only the largest more-energetic eddies are resolved, then the model is called a large-eddy simulation model.

Predictability, however, must be split into two categories: (1) ***pattern predictability*** and (2) ***statistical results from pattern forecasts***. Studies have suggested that individual patterns or structures, whether it be a synoptic-scale cyclone or a turbulent-scale eddy, can be accurately predicted in an Eulerian model out to times no greater than the Lagrangian lifetime of the pattern or structure (Stull, 1985). For example, if we were to take our hypothetical numerical model and initialize it with the exact observed wind field including the precise variations in wind field associated with each of the turbulent eddies present, then we could anticipate forecasting the evolution of those initialized eddies out to about 5 to 15 min for the thermals, but only out to a few seconds for the smaller-sized eddies. This is pattern or structure predictability.

If we continue the forecast beyond the limit of accurately forecast deterministic patterns, then we will continue to generate eddies and thermals in the model, except these eddies will be happening at different times and places with different intensities than the true observed eddies. If the model was designed correctly, then the statistics (TKE,

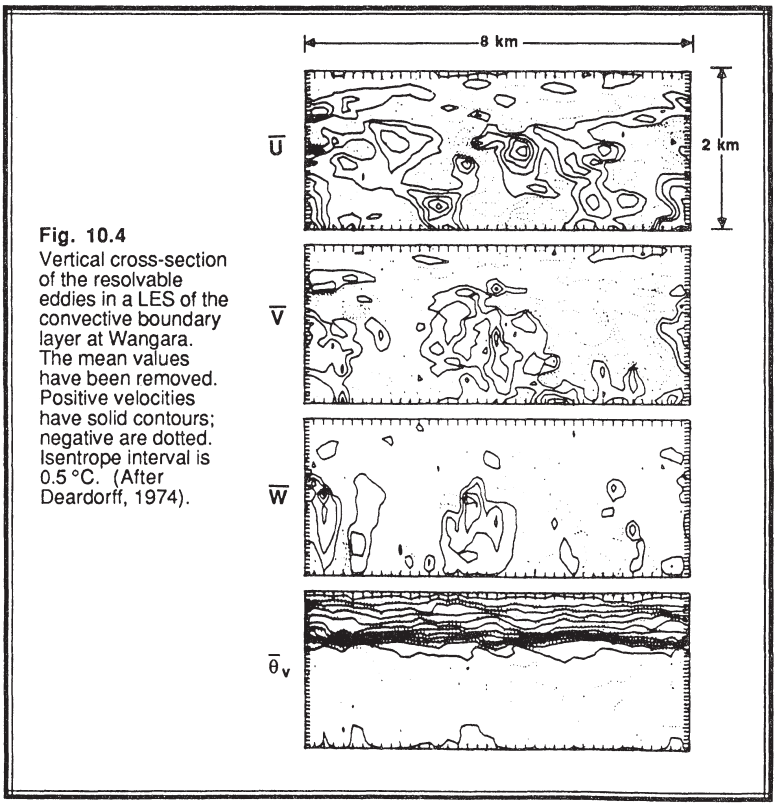

Fig. 10.4
Vertical cross-section of the resolvable eddies in a LES of the convective boundary layer at Wangara. The mean values have been removed. Positive velocities have solid contours; negative are dotted. Isentrope interval is 0.5 °C. (After Deardorff, 1974).

turbulent fluxes, etc.) calculated from this forecast will be close to those observed. In other words, we will have accurate statistical results from deterministic pattern forecasts, even though the simulated patterns themselves do not have a one-to-one correspondence with the true patterns. Such statistical accuracy can be maintained for days of simulated turbulence forecasts.

For the remainder of this section we will focus on such statistically-accurate pattern forecasts. In fact, most modelers do not have observed wind and temperature fields with a resolution that includes the effects of all the observed eddies. Instead, they (1) initialize the model with the observed mean wind and temperature and mean boundary forcings, (2) "kick" start turbulent motions by imposing a pseudo-random temperature and/or velocity perturbations on the mean field for just the first one or two timesteps, and (3) hope that statistically realistic structures develop. Thus, there is no intention of making precise pattern forecasts, even over the first few minutes.

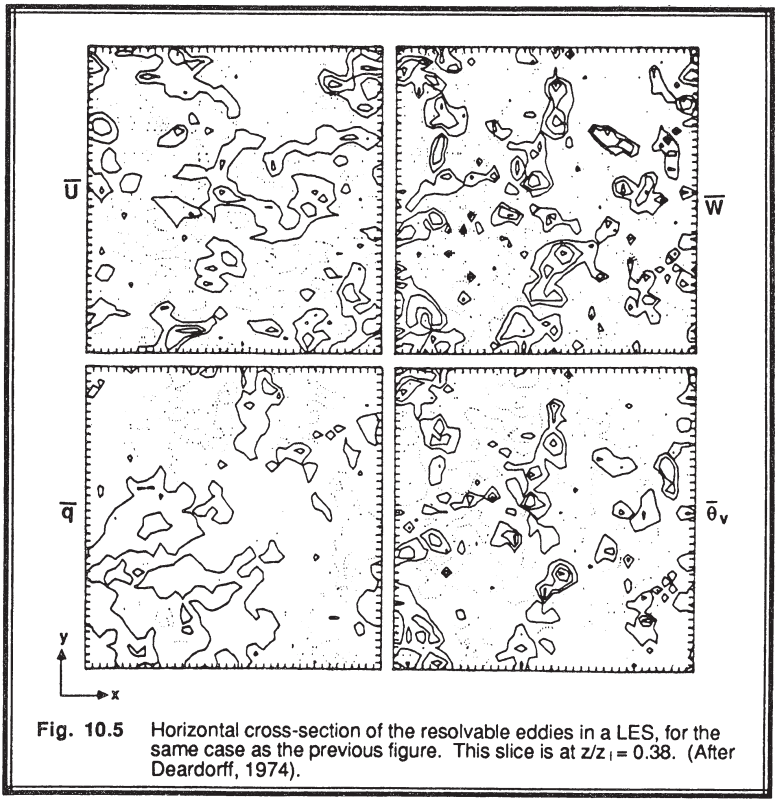

Fig. 10.5 Horizontal cross-section of the resolvable eddies in a LES, for the same case as the previous figure. This slice is at $z/z_i = 0.38$. (After Deardorff, 1974).

Because of computer limitations, numerical models are limited to a finite number of grid points or wavenumbers for all practical purposes, instead of the infinite number of points in our hypothetical model. Thus, each modeled grid point must represent the average of a small volume of fluid in its immediate neighborhood. Given a grid point spacing of Δx, we know from the Nyquist frequency arguments in the previous chapter that the smallest feature that can be represented has a size of $2\Delta x$. Features of this size and larger are said to be ***resolved*** by the model, and represent ***grid-scale*** phenomena. Features smaller than $2\Delta x$ are ***sub-grid scale***; their affect on the flow must be parameterized because they can not be explicitly resolved.

Deardorff (1972) pioneered the use of such numerical models for boundary layer simulations, while Wyngaard and Brost (1984) and Moeng (1984a, 1986, 1987) have updated versions. Computer limitations in those models restricted grid-point spacings to about 150 m in the horizontal and 50 m in the vertical, within a domain of (x,y,z) = (5,5,3) km. These models were called ***large-eddy simulation*** (LES) models (see Fig 10.3), because only the largest-size turbulent eddies could be resolved. At each of the over 60,000 grid points in a typical model, forecasts were made for θ, q, u, v and w, with additional diagnostic equations for p. At the time this text was written, such a model would take about an hour of computer CPU time for each hour simulated. The subgrid-scale turbulence was parameterized in these models using schemes ranging from K-theory to second-order closure.

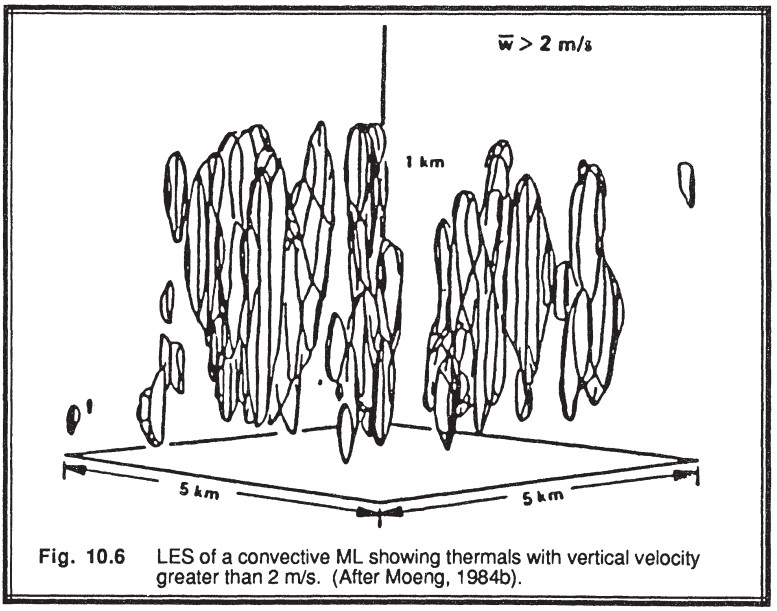

Fig. 10.6 LES of a convective ML showing thermals with vertical velocity greater than 2 m/s. (After Moeng, 1984b).

By averaging over a series of horizontal planes, we can compute mean vertical profiles of various variables. For ***area-averaged*** turbulence statistics such as TKE or fluxes, the subgrid parameterized component must be added to the resolvable-scale values to yield the total value at any height. Such area averages are analogous to area averages produced from remote sensor output, assuming the sensor can scan a volume. In a similar way, statistics can be found by volume-averaging over limited subvolumes of the domain. These ***volume averages*** are more closely related to the volume averages of real data that to the ensemble averages discussed in Chapter 2.

Convective Mixed Layer. Figs 10.4 and 5 show examples of vertical and horizontal cross sections through Deardorff's LES model, where resolvable-scale turbulent structures that look like thermals are revealed. Fig 10.6 shows Moeng's (1984b) simulation of thermal updrafts in a convective boundary layer, while Fig 10.7 shows an analysis of the temperature structure of thermals. It is obvious that these models forecast pseudo-random turbulent structures in both space and time. In fact, the variation of temperature or velocity with time at any one grid point within the turbulent domain would exhibit a trace similar to Fig 2.1. An example of the area-averaged mean potential temperature, humidity, and TKE profiles are shown in Fig 10.8.

Many of the figures in Chapters 3-5 are composites of real data with numerical simulations, because the simulations filled in the gaps that were not (or could not be) measured in the field.

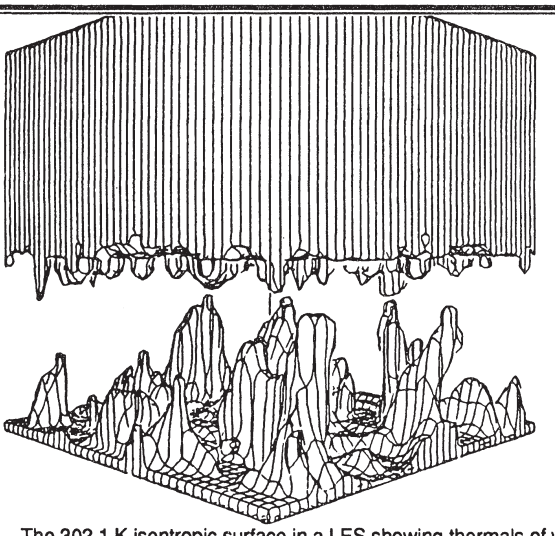

Fig. 10.7 The 302.1 K isentropic surface in a LES showing thermals of warm air rising through a convective ML up toward a warm capping inversion. (After Moeng, 1986).

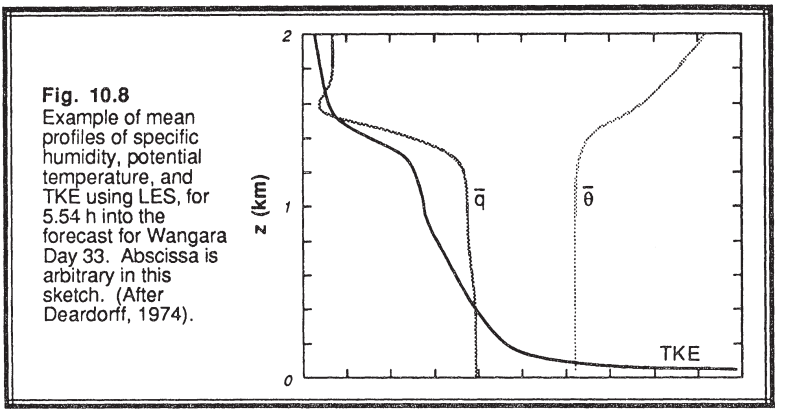

Fig. 10.8
Example of mean profiles of specific humidity, potential temperature, and TKE using LES, for 5.54 h into the forecast for Wangara Day 33. Abscissa is arbitrary in this sketch. (After Deardorff, 1974).

Neutral Boundary Layer. Mason and Thomson (1987) have used LES to simulate structures in neutral boundary layers. Their model shows that smaller eddies dominate near the surface, while larger eddies are more important aloft. These large eddies are often elongated in the direction of the shear vector.

Stable Boundary Layer. Large eddies are suppressed by static stabilities, leaving only the smaller eddies that cannot be resolved by a LES model (as of the date this book was written). Thus, we will have to wait for better computers before we can expect successful LES of the SBL.

10.6.2 Laboratory Tank

When a fluid such as water is used to simulate atmospheric turbulence, one must take care to insure that the simulation has the same dimensionless scales as the atmosphere (Willis and Deardorff, 1974; Deardorff and Yoon, 1984). The atmosphere is a high Reynolds number flow — so high that the Reynolds number is not a governing parameter. However, the dimensions of some laboratory tanks are small enough that the Reynolds number is not very large — meaning that viscosity causes the tank flow to differ from the atmospheric flow. Other numbers, such as the Rayleigh, Nussult, Richardson and Prandtl numbers should be considered. The surface heating rate or mechanical stirring rate must be chosen to make the proper convective or friction velocity scales, respectively, given the higher density of the water.

Convective Turbulence: A large number of simulations of convective mixed layers have been performed by Willis and Deardorff (1974; Deardorff and Willis, 1985, 1987) using water as the working medium. They used a tank that was approximately cubical, with dimensions of about 1 m on each side. The tank would initially be filled with cooler water on the bottom, smoothly varying to warmer water at the top, thereby

simulating a stably stratified temperature inversion as is typically observed in the real atmosphere in the early mornings. The bottom of the tank was a metal plate that could be heated to generate convection in the tank. Convection has been induced by other investigators using other techniques such as cooling water below 4°C, or introducing denser brines into the top of the tank.

Using a variety of dyes and neutrally buoyant oil droplets, they could photogrametrically analyze the evolution, turbulent structure, and dispersive characteristics of the mixed layer. Illuminating the tank with thin planes of light allowed cross sections to be photographed, and illuminating the top part of the tank simulated features similar to small cumulus clouds. In situ measurements of temperature and velocity were also made with probes that could be slowly moved through the fluid. This technique was extended to study buoyancy waves and forced convection. Some of their discoveries concerning the entrainment zone and dispersion were later verified in the real atmosphere.

Mechanical Turbulence: The simulation of realistic shear-driven turbulent flows in the laboratory has proved to be very difficult. Circular or racetrack-shaped annulus tanks are often employed to avoid the acceleration/deceleration problems of a long-straight tank. Regardless of whether the fluid is put into motion by pumps or whether the boundaries are moved relative to the fluid, there appear to be major boundary problems associated with fluid circulating around the annulus (Scranton and Lindberg, 1983; Deardorff and Yoon, 1984). Some of the published results from such shear-driven flows are of questionable quality.

For some ocean mixed layer simulations, mechanical turbulence has been generated in tanks using oscillating grids. These mechanically stir the fluid. Although such stirring might be an approximate representation of the breaking of waves and wind-induced mixing at the top of the ocean mixed layer, it is difficult to find an analogy in the atmospheric mixed layer.

Stable Stratification: The non-turbulent flow of stably stratified fluid over terrain and around obstacles has been simulated using ***towing tanks***. These are long narrow tanks filled with stably stratified (using salt brine or temperature to vary the density) water, where the mean water flow is zero. A scale model of the terrain or obstacle is then placed upside-down in the top of the tank and towed along the tank's length, while tracer dies are released from tiny holes in the model. Cameras translating at the same speed as the model record the flow, which then appears as fluid moving past the obstacle when the films are played back. These tanks have been particularly valuable for pollution dispersion studies.

10.6.3 Wind Tunnel

Wind tunnels have the advantage of using air as the working medium. A disadvantage is that it is difficult to stratify the flow. For neutral stratification, wind tunnels have been used successfully to study dispersion and flow over hills and around obstacles. In

particular, complex physical models of buildings, smoke stacks, and terrain can be constructed and placed in the wind tunnel. Such a wind tunnel simulation is often superior to the corresponding numerical simulation, which is often too difficult to design.

One variation on the wind tunnel is the wind-wave tunnel, where the bottom half of the channel is filled with water and the top is air. This is useful in studying air-sea interaction. There are also many other good uses for wind tunnels in meteorology, such as calibrating anemometers.

10.7 Analysis Methods

Values of mean wind, temperature and humidity can be measured directly. Fluxes, TKE, and dissipation rates can be calculated in a variety of ways, as we discuss in detail here.

10.7.1 Eddy Correlation Method — for various statistical moments such as fluxes, variances, TKE

Fast-response measurements of state variables generate time series of data that we can statistically analyze; however, problems with the series must be fixed before performing the eddy-correlation calculations. Sometimes there are spikes in the data (unrealistically large or small values) associated with nonmeteorological events (bug strikes on the sensor, voltage surges in the power supply). These spikes must be removed and replaced with good or bogus data. The data should be detrended (or at least demeaned) and high-pass filtered to remove wavelengths longer than about 1/3 to 1/5 of the length of the series. This latter procedure insures that enough complete cycles of the retained wavelengths are averaged to yield significant statistics. If spectra are to be found, then additional conditioning is sometimes necessary, as described in Chapter 8. Finally, we are left with a "clean" series that can be used in the eddy-correlation analysis.

The first step in the eddy-correlation process is to calculate the perturbation values of the data points. For example, given a time series of measurements of potential temperature, we can subtract the mean potential temperature from each data point to yield the time series of perturbations [e.g., $\theta'(t)$, $\theta'(t+\Delta t)$, $\theta'(t+2\Delta t)$, $\theta'(t+3\Delta t)$, ...]. We can similarly find a time series of vertical velocity perturbations [e.g., $w'(t)$, $w'(t+\Delta t)$, $w'(t+2\Delta t)$, $w'(t+3\Delta t)$, ...]. Multiplying the respective values together yields a time series of $w'\theta'$: [e.g., $w'\theta'(t)$, $w'\theta'(t+\Delta t)$, $w'\theta'(t+2\Delta t)$, $w'\theta'(t+3\Delta t)$, ...]. The average of this series, $\overline{w'\theta'}$, is the definition of kinematic turbulent heat flux in the vertical, as was shown in Chapter 2.

Once time series of θ', q', u', v', and w' are calculated from a data set, we can find via simple multiplication and averaging quantities such as fluxes [e.g., $\overline{u'w'}$, $\overline{w'q'}$,

$\overline{w'\theta'}$], variances [e.g., $\overline{w'^2}$, $\overline{q'^2}$, $\overline{u'^2}$, $\overline{\theta'^2}$], turbulence kinetic energy [TKE = $0.5 \cdot (\overline{u'^2} + \overline{v'^2} + \overline{w'^2})$], fluxes of variances [e.g., $\overline{w'q'^2}$, $\overline{w'\theta'^2}$, $\overline{u'^2 w'}$, $\overline{w'^3}$], fluxes of fluxes [e.g., $\overline{w'^2\theta'}$, $\overline{w'^2 q'}$, $\overline{u' w'^2}$], fluxes of energies [e.g., $\overline{w'e} = 0.5 \cdot \overline{w'(u'^2 + v'^2 + w'^2)}$], and higher moments [e.g., $\overline{w'^2\theta'^2}$, $\overline{u'^3 q'}$, $\overline{w'^4}$].

An advantage of this method is that it is direct and simple, and fluxes can be calculated at whatever height or location that the original time series was measured. A disadvantage is that expensive fast-response sensors must be used. If slower response sensors were substituted, the perturbation values will be filtered by the instrument response to smaller magnitudes, resulting in incorrect fluxes and other eddy correlations. Another disadvantage is that errors in the original series compound themselves as higher and higher moments are calculated, so that by the third or fourth moments the noise (error) is as large or larger than the signal.

In Sections 2.6 and 3.2.5 we gave only the briefest overview of the relationship between actual sensible heat flux, $\tilde{Q}_H$, and the kinematic flux, $\overline{w'\theta'}$. The precise relationship is (Brook, 1978; Riehl, et al., 1978):

$$\tilde{Q}_H = \bar{\rho}\, \overline{w'(C_p T)'} \qquad (10.7.1a)$$

But the value of specific heat for air, C_p, varies with humidity approximately as

$$C_p = C_{pd}\,(1 + 0.84\, q) \qquad (10.7.1b)$$

where $\{[C_{p\ \text{water vapor}} - C_{pd}] / C_{pd}\} = 0.84$. Combining these two equations and neglecting the higher-order terms yields:

$$\tilde{Q}_H \cong \bar{\rho}\, C_{pd} \left(\overline{w'T'} + 0.84\, \bar{T}\, \overline{w'q'} \right) \qquad (10.7.1c)$$

The last term can cause about a 10% change in the estimate of sensible heat flux compared to that using only the dry specific heat, and thus should not be neglected. The corresponding expression for latent heat flux is:

$$\tilde{Q}_E = \bar{\rho}\, L_v\, \overline{w'q'} \qquad (10.7.1d)$$

10.7.2 Flux-Profile Relationship Method — for surface fluxes

In Section 9.7.5 the Businger-Dyer relationships between the magnitude of the surface flux and the shape of the vertical profile of a mean variable in the surface layer were presented. To use this technique, either iterative or nonlinear regression techniques must be used to estimate the flux that yields the best fit of the theoretical mean profile to the data. For statically non-neutral situations, both the wind and temperature profiles must be simultaneously fit, because the Obukhov length that appears in the theoretical equations for each of those profiles is a function of both $\overline{w'\theta'}_s$ and u_*. Although this iterative approach is somewhat tricky, it nevertheless allows calculation of fluxes from measurements of mean-variable profiles.

Advantages of flux-profile methods are that less-expensive slow-response sensors can be used to measure the mean profiles, from which fluxes are then inferred. Disadvantages are that the relationship between flux and mean profile is an empirical parameterization. Also, sometimes the shape of the profile is altered by other factors, such as change in roughness or displacement distance. Another disadvantage is that only fluxes at the surface can be found, because surface-layer similarity is used.

Although the Businger-Dyer flux profile relationships are preferred for this calculation, one could also try to use K-theory. Thus, measurement of the temperature difference between two heights could be used to estimate the heat flux at the average height, for example,

$$\overline{w'\theta'} = -K_H \Delta\bar{\theta} / \Delta z \tag{10.7.2}$$

assuming that the value for K is known. This offers the advantage that fluxes can be determined at any height where the local gradient of the corresponding mean variable can be measured. Disadvantages include the fact that the K-theory approach assumes local down-gradient diffusion, and neglects the contribution to flux from larger eddies. We do not recommend use of the K-theory method because of the uncertainty about the value of K.

10.7.3 Profile Similarity Method — for fluxes

Using a K-theory approximation like (10.7.2) for two different fluxes, we can write the ratio of fluxes as:

$$\frac{\overline{w'q'}}{\overline{u'w'}} = \frac{-K_E \ (\Delta\bar{q}/\Delta z)}{-K_m \ (\Delta\bar{U}/\Delta z)} = \left(\frac{K_E}{K_m}\right) \frac{\Delta\bar{q}}{\Delta\bar{U}} \tag{10.7.3}$$

Thus, if only one of the fluxes is known from some other measurement technique, then the second flux can be estimated by simply comparing the ratio of the differences of the two mean variables across some height. Furthermore, even though the exact value for K is not well known, the ratio of K values is more well known. For example, it is often

assumed that K for all scalars and heat are equal to each other, while $K_m = 0.74\ K_H$ for statically neutral conditions (see Section 9.7.5).

Advantages of this approach are that simple mean measurements at two different heights and knowledge of any one flux is sufficient to determine the other fluxes. This is particularly valuable for moisture flux, which is notoriously difficult to measure directly. The disadvantage is that one of the fluxes must still be measured by other means.

10.7.4 Bowen Ratio Method — for surface fluxes

An equation like (10.7.3) can be written for the Bowen ratio:

$$\beta = \frac{Q_H}{Q_E} = \frac{C_p K\, \partial\bar{\theta}/\partial z}{L_v K\, \partial\bar{q}/\partial z} = \gamma \frac{\Delta\bar{\theta}}{\Delta\bar{q}} \qquad (10.7.4a)$$

We are neglecting for simplicity the variation of C_p with humidity in the development that follows; a more accurate approach should employ (10.7.1c). At the surface, we can relate Q_H and Q_E via the energy balance (7.5): $(-Q^*_s + Q_G) = Q_H + Q_E$. These two equations can be solved for Q_H and Q_E:

$$Q_H = \frac{-Q^*_s + Q_G}{\frac{\Delta\bar{q}}{\gamma\Delta\bar{\theta}} + 1} \qquad \text{and} \qquad Q_E = \frac{-Q^*_s + Q_G}{\frac{\gamma\Delta\bar{\theta}}{\Delta\bar{q}} + 1} \qquad (10.7.4b)$$

Thus, if the simple measurements of $\Delta\bar{q}$ and $\Delta\bar{\theta}$ are made in the surface layer from sensors at two different heights on a mast, and if the net radiation is measured and the ground flux is measured or estimated, then we can find the surface sensible and latent heat fluxes.

The advantages of this approach are that it is simple, and the resulting fluxes balance the surface energy budget by definition. The disadvantage is that there are times (such as sunrise and especially sunset) when $\Delta\bar{q}$ or $\Delta\bar{\theta}$ are small, causing equations (10.7.4b) to blow up and give unrealistic results. At other times during the day or night, this approach appears to work well.

10.7.5 Spectral Method — for dissipation rate

Dissipation rates are difficult to measure directly, but they are easy to infer from similarity approaches. From Section 9.9.1 recall that $S(\kappa) = \alpha_k\, \varepsilon^{2/3}\, \kappa^{-5/3}$ in the inertial subrange. This can be solved for ε using the following steps:

1) Make fast response measurements of velocity to get a time series.
2) Calculate the FFT of the time series, from which spectral densities, S, can be found.
3) Plot the spectra on a log-log graph.
4) Identify the inertial subrange: that portion of the spectrum that exhibits a -5/3 slope.
5) Fit a straight line with -5/3 slope to this portion of the graph.
6) Pick any point on this line, and record the S and κ values of that point
7) Solve for ε using: $\varepsilon = 0.49\, S^{3/2}\, \kappa^{5/2}$.

The prime reason for using this method is that it is the only way to find dissipation without using structure functions. A disadvantage is that typical atmospheric spectra has considerable variability, even in the inertial subrange. This variability translates into error bars on the estimate of ε.

10.7.6 Structure Function Method — for dissipation rate

Using (8.3.1d), we can easily solve for dissipation rate: $\varepsilon = 0.35\, (c_{v2})^{3/2}$. An advantage is that measurements can be made at points in the atmosphere distant from the sensor, but the corresponding disadvantage is that the remote sensors necessary to do this are somewhat expensive. Similar methods can be used to estimate ε_θ.

10.7.7 Residual Method — for estimating terms that are difficult to measure

Some of the higher moments and pressure terms are difficult to measure directly. However, if a conservation or budget equation contains these terms and if all the other terms in the equation can be measured by other techniques, then the unknown terms can be found by making the equation balance. The advantage is that there may be no known alternative for measuring some of these terms. The disadvantage is that all of the errors from the known terms accumulate and are added into the estimate of the unknown term. Most studies that have used this method make an appropriate disclaimer that the residual values include errors as well as the term of interest.

Suppose, for example, that we wish to calculate the term $\overline{w'p'}$. After searching through our catalog of budget equations, we find the TKE equation: (5.1b). Using eddy correlation methods for terms I-V and spectral methods for term VII, we can solve for $\overline{w'p'}$ as a residual (Wyngaard and Coté, 1971).

In another example, Gal-Chen and Kropfli (1984) have used Doppler radar data to estimate pressure perturbation and buoyancy flux. This is a good trick, because the Doppler radar measures only velocities. Their approach was to use a number of budget equations together to eliminate most of the terms that could not be measured by their one

sensor. Needless to say, a number of simplifying assumptions (e.g., steady state, anelastic, isotropic, etc.) must be made.

Wilczak and Businger (1984) used the momentum equations along with assumptions of large-eddy ramp structures, stationarity, homogeneity, Boussinesq, and others to calculate pressure perturbations, using only temperature and velocity measurements from the BAO tower.

10.7.8 Similarity Methods

We have already described a variety of similarity methods, including dissipation rate estimation using spectral similarity in the inertial subrange, and the Businger-Dyer flux-profile similarity. Many other similarity relationships exist between various boundary layer variables that can be employed to solve for unknowns.

For example, we know the similarity shape for vertical velocity variance as a function of scaled height in the mixed layer (9.6.3c): $\overline{w'^2}/w_*^2 = 1.8\,(z/z_i)^{2/3}\,(1 - 0.8\,z/z_i)^2$. We could measure $\overline{w'^2}$ at any height in the mixed layer, and if we also know the mixed layer depth z_i, then we can solve for the surface buoyancy flux $\overline{w'\theta_v'}_s$ because it appears in the w_* scaling velocity. It's hard to believe, but by making velocity measurements 1 km above the surface we can infer surface buoyancy flux, without even measuring temperature.

An advantage is that a large number of similarity relations exist, allowing a large variety of variables to be estimated this way. The disadvantage is that the similarity approach is empirical, based on best fits of arbitrary curves to previously measured data rather than being based on conservation equations derived from first principles.

10.7.9 Examples

Problem: Given the following measurements in the surface layer:

$\overline{w'T'} = 0.2$ K m/s, $\overline{w'q'} = 0.1$ (g/kg)·(m/s), $\bar{T} = 300$ K, $-\tilde{Q}^*_s + \tilde{Q}_G = 546$ W/m^2,

$\Delta\bar{\theta} = -2$ K, $\Delta\bar{q} = -0.818$ g/kg, $\Delta\bar{U} = 5$ m/s, $c_{v2} = 0.4$ m$^{4/3}$ s^{-2}, and

$S(\kappa) = 0.015$ m^3 s^{-2} at $\kappa = 6.28$ m^{-1}. Find:

(a) $\tilde{Q}_H$ and $\tilde{Q}_E$ in W/m^2 using the eddy correlation method.

(b) $\tilde{Q}_H$ and $\tilde{Q}_E$ in W/m^2 using the Bowen ratio method.

(c) $\overline{u'w'}$ using the profile similarity method.

(d) ε using the structure function method.

(e) ε using the inertial subrange (spectral) method.

Solution: (a) We must utilize (10.7.1c and d), to find the fluxes. We can use ρC_{pd} = 1200 (W/m^2)/(K m/s) and ρL_v = 2760 (W/m^2)/[(g/kg)·(m/s)] to conveniently convert between dynamic and kinematic units. Remembering to first convert the moisture flux to units of (g/g)(m/s) for the sensible heat flux equation, we find:

$$\tilde{Q}_H = \bar{\rho}\, C_{pd} \left(\overline{w'T'} + 0.84\, \bar{T}\, \overline{w'q'} \right)$$

$$\tilde{Q}_H = (1200) \cdot [0.2 + 0.025] = 270 \text{ W/m}^2$$

and

$$\tilde{Q}_E = (2760) \cdot [0.1] = 276 \text{ W/m}^2$$

(b) Using (10.7.4b) and assuming that the psychrometric constant is 0.4 (g/kg)K^{-1}:

$$\tilde{Q}_H = \frac{-\tilde{Q}_s^* + \tilde{Q}_G}{\frac{\Delta\bar{q}}{\gamma\,\Delta\bar{\theta}} + 1} \quad \text{and} \quad \tilde{Q}_E = \frac{-\tilde{Q}_s^* + \tilde{Q}_G}{\frac{\gamma\,\Delta\bar{\theta}}{\Delta\bar{q}} + 1}$$

$$\tilde{Q}_H = (546) \,/\, \{[-0.818/(-2 \cdot 0.4)]+1\} = 270 \text{ W/m}^2$$

$$\tilde{Q}_E = (546) \,/\, \{[(-2 \cdot 0.4)/(-0.818)]+1\} = 276 \text{ W/m}^2$$

(c) Assuming for simplicity that the ratio of eddy diffusivities = 0.74 (which is not quite true in statically unstable conditions), and using (10.7.3) we find that:

$$\overline{u'w'} = \overline{w'\theta'}\, \frac{K_m\, \Delta\bar{U}}{K_H\, \Delta\bar{\theta}} = (0.2)\,(0.74)\left(\frac{5}{-2}\right) = -0.37 \text{ m}^2\text{s}^{-2}$$

(d) $$\varepsilon = (0.5\, c_{v2})^{3/2} = (0.2)^{3/2} = 0.089 \text{ m}^2\text{s}^{-3}$$

(e) $$\varepsilon = 0.49 \cdot S^{3/2}\, \kappa^{5/2} = (0.49)\,(0.015)^{3/2}\,(6.28)^{5/2} = 0.089 \text{ m}^2\text{s}^{-3}$$

Discussion: As demonstrated above, there are often a variety of methods that can be used to calculate fluxes and other variables. We recommend that field experiments utilize several methods to estimate each flux. Invariably, the different methods will give different answers, but the overall result will give the researcher a better estimate of the true answer, and will also provide an estimate of the errors.

10.8 References

André, J.-C., J.-P. Goutorbe, and A. Perrier, 1986: HAPEX-MOBILHY, a hydrologic atmospheric pilot experiment for the study of water budget and evaporation flux at the climatic scale. *Bull. Am. Meteor. Soc.*, **67**, 138-144.

André, J.-C., J.-P. Goutorbe, and A. Perrier, 1988: HAPEX-MOBILHY: first results from the special observing period. *Annales Geophysicae* (in press).

André, J.C., and P. Lacarrere, 1980: Simulation numérique détaillée de la couch limite atmosphérique, compasaison avec le situation des 2 er 3 Juilles 1977 à Voves. *La Météorologie VI*, **22**, 5-49.

AMS, 1985: Project to find causes of destructive winter storms (GALE). *Bull. Am. Meteor. Soc.*, **66**, 705-706.

Betts, A.K. and R.D. Miller, 1975: *VIMMHEX-1972 Rawinsonde Data.* Dept. of Atmos. Sci., Colorado State Univ. Fort Collins. 150pp.

Brook, R.R., 1978: The influence of water vapor fluctuations on turbulent fluxes. *Bound.-Layer Meteor.*, **15**, 481-487.

Changnon, S.A. (Ed.), 1981: *METROMEX: A Review and Summary.* Meteor. Monographs, 18, No.40. Am. Meteor. Soc. 181pp.

Clarke, R.H., A.J. Dyer, R.R. Brook, D.G. Reid and A.J. Troup, 1971: *The Wangara Experiment: Boundary Layer Data.* Div. of Meteor. Phys. Tech. Paper No. 19. CSIRO, Melbourne. 350pp.

Clarke, R.H. and R.R. Brook (Eds.), 1979: *The Koorin Expedition, Atmospheric Boundary Layer Data over Tropical Savannah Land.* Dept. of Sci. and the Environ., Bureau of Meteor. Australian Gov. Publ. Service, Canberra. 359pp.

Cunning, J.B., 1986: The Oklahoma-Kansas Preliminary Regional Experiment for STORM-Central. *Bull. Am. Meteor. Soc.*, **67**, 1478-1486.

Deardorff, J.W., 1972: Numerical investigation of neutral and unstable planetary boundary layers. *J. Atmos. Sci.*, **29**, 91-115.

Deardorff, J.W., 1974: Three-dimensional numerical study of turbulence in an entraining mixed layer. *Bound.-Layer Meteor.*, **7**, 199-226.

Deardorff, J.W. and G.E. Willis, 1985: Further results from a laboratory model of the convective planetary boundary layer. *Bound.-Layer Meteor.*, **32**, 205-236.

Deardorff, J.W. and G.E. Willis, 1987: Turbulence within a baroclinic laboratory mixed layer above a sloping surface. *J. Atmos. Sci.*, **44**, 772-778.

Deardorff, J.W. and S.-C. Yoon, 1984: On the use of an annulus to study mixed layer entrainment. *J. Fluid Mech.*, **142**, 97-120.

DeHeer-Amissah, A., U. Högström, and A. Smedman-Högström, 1981: Calculation of sensible and latent heat fluxes, and surface resistance from profile data. *Bound.-Layer Meteor.*, **20**, 35-49.

Desbraux, G. and A. Weill, 1986: Mean turbulent properties of the stable boundary layer observed during the COAST experiment. *Atmos. Res.*, **20**, 151-164.

Gal-Chen, T. and R.A. Kropfli, 1984: Buoyancy and pressure perturbations derived from dual-Doppler radar observations of the planetary boundary layer: applications for

matching models with observations. *J. Atmos. Sci.*, **41**, 3007-3020.

Gryning, S.E., 1985: The Øresund experiment - A Nordic mesoscale dispersion experiment over a land-water-land area. Bull. Am. Meteor. Soc., 66, 1403-1407.

Harris, R., 1987: Amazon boundary layer experiment. Airborne Science Newsletter, 87-2 (June). NASA Airborne science program office. 2

Hill, K, G.S. Wilson and R.E. Turner, 1979: SESAME News: NASA's participation i the AVE-SESAME '79 program. *Bull. Am. Meteor. Soc.*, **60**, 1323-1329.

Hoeber, H., 1982: KONTUR: Convection and turbulence experiment: Field phase Report. Hamburger Geophysikalische Einzelschriften, Reihe B, No. 1.

Högström, U., 1974: A field study of the turbulent fluxes of heat, water vapour and momentum at a typical agricultural site. *Quart. J. Roy. Meteor. Soc.*, **100**, 624-639.

Hooke, W.H. (Ed.), 1979: *Project PHOENIX, The September 1978 Field Operation.* NOAA/ERL Wave Propagation Lab. & NCAR. NCAR Publications Office, P.O. Box 3000, Boulder. 281pp.

Izumi, Y., 1971: *Kansas 1968 Field Program Data Report.* Air Force Cambridge Res. Lab. AFCRL-72-0041. Environ. Res. Paper No. 379, Hanscom AFB, MA . 79pp.

Izumi, Y., and J.S. Caughey, 1976: *Minnesota 1973 Atmospheric Boundary Layer Experiment Data Report.* Air Force Cambridge Research Lab. AFCRL-TR-76-0038, Environ. Res. Papers No. 547, Hanscom AFB, MA 01731. 28pp.

Katsaros, K.B., S.D. Smith and W.A. Oost, 1987: HEXOS - Humidity exchange over the sea. A program for research on water-vapor and droplet fluxes from sea to air at moderate to high wind speeds. *Bull. Am. Meteor. Soc.*, **68**, 466-476.

Keuttner, J.P. and J. Holland, 1969: The BOMEX project. *Bull. Am. Meteor. Soc.*, **50**, 394-402.

Keuttner, J.P., and D.E. Parker, 1976: GATE: Report on the field phase. *Bull. Am. Meteor. Soc.*, **57**, 11-30.

Knight, C.A. (Ed.), 1982: The cooperative convective precipitation experiment (CCOPE), 18 May-7 August 1981. *Bull. Am. Meteor. Soc.*, **63**, 386-398.

KONTUR Results, 1985: Collection of papers, *Beitr. Phys. Atmosph.*, **58**, 1-52.

Kraus, H. , 1982: PUKK - A mesoscale experiment at the German North Sea Coast. *Beitr. Phys. Atmosph.*, **55**, 370-382.

Lenschow, D.H. (Ed.), 1986: *Probing the Atmospheric Boundary Layer.* Amer. Meteor. Soc., Boston, MA. 269pp.

Lenschow, D.H., and E.M. Agee, 1976: Preliminary results from the air mass transformation experiment (AMTEX). *Bull. Am. Meteor. Soc.*, **57**, 1346-1355.

Lenschow, D.H. and B.B. Stankov, 1986: Length scales in the convective boundary layer. *J. Atmos. Sci.*, **43**, 1198-1209.

Lettau, H.H. and B. Davidson, 1957: *Exploring the Atmosphere's First Mile, Proceedings of the Great Plains Field Program 1 August to 8 September 1953, O'Neill, Nebraska. Vols I and II.* Pergamon Press, NY. 578pp.

Lilly, D., 1984: NCAR, NOAA Oklahoma University scientists gear up for field project. News and Notes. *Bull. Am. Meteor. Soc.*, **65**, 721.

Mason, P.J. and D.J. Thomson, 1987: Large eddy simulations of the neutral-static stability planetary boundary layer. *Quart. J. Roy. Meteor. Soc.*, **113**, 413-443.

Moeng, C.-H., 1984a: A large-eddy simulation model for the study of planetary boundary-layer turbulence. *J. Atmos. Sci.*, **41**, 2052-2062.

Moeng, C.-H., 1984b: Eddies in the atmosphere. *Annual Report, Fiscal Year 1983, National Center for Atmospheric Research.*, **NCAR/AR-83**, 57-58.

Moeng, C.-H., 1986: Large-eddy simulation of a stratus-topped boundary layer, Part I: Structure and budgets. *J. Atmos. Sci.*, **43**, 2886-2900.

Moeng, C.-H., 1987: Large-eddy simulation of a stratus-topped boundary layer, Part II: Implications for mixed-layer modeling. *J. Atmos. Sci.*, **44**, 1605-1614.

Monna, W.A.A., and J.G. Van der Vliet, 1987: Facilities for research and weather observations on the 213 m tower at Cabauw and at remote locations. KNMI Scientific Report WR-87-5, De Bilt, The Netherlands.

Negri, A.J., 1982: SESAME News: Cloud-top structure of tornadic storms on 10th April 1979 from rapid scan and stereo satellite observations. *Bull. Am. Meteor. Soc.*, **63**, 1151-1159.

Nieuwstadt, F.T.M., 1984: The turbulent structure of the stable, nocturnal boundary layer. *J. Atmos. Sci.*, **41**, 2002-2216.

Nieuwstadt, F.T.M. and R.A. Brost, 1986: The decay of convective turbulence. *J. Atmos. Sci.*, **43**, 532-546.

Noonkester, V.R., 1979: A technique for coding boundary layer echoes from surface-based remote sensors. *Bull. Am. Meteor. Soc.*, **60**, 20-27.

Reihl, H., G. Greenhut, and B.R. Bean, 1978: Energy transfer in the tropical subcloud layer measured with DC-6 aircraft during GATE. *Tellus*, **30**, 524-536.

Scranton, D.R. and W.R. Lindberg, 1983: An experimental study of entraining, stress-driven, stratified flow in an annulus. *Phys. Fluids*, **26**, 1198-1205.

Smedman-Högström,A., and U. Högström, 1973: The Marsta micrometeorological field project. Profile measurement system and some preliminary data. *Bound.-Layer Meteor.*, **5**, 259-273.

Stage, S.A. and R.A. Weller, 1986: The frontal air-sea interaction experiment (FASINEX); Part II: Experimental plan. *Bull. Am. Meteor. Soc.*, **67**, 16-20.

Stull, R.B., 1985: Predictability and scales of motion. *Bull. Am. Meteor. Soc.*, **66**, 432-436.

Weill, A., F. Baudon, G. Resbraux, C. Mazaudier, C. Klapisz and A.G.M. Driedonks, 1985: A mesoscale shear-convective organization and boundary-layer modification: an experimental study performed with acoustic Doppler sounders during the COAST experiment. *Proceedings of the Second Conference on Mesoscale Processes*, Am. Meteor. Soc., June 3-7, 1985, Univ. Park, PA.

Weill, A., C. Mazaudier, F. Baudin, C.Klapisz, F. Leca, M. Masmoudi, D. Vidal Madjar, R. Bernard, O. Taconet, B.S. Gera, A. Sauvaget, A. Druilhet, P. Durand, J.Y. Caneill, P. Mery, G. Dubosclard, A.C.M. Beljaars, W.A.A. Monna, J.G. Van der Vliet, M. Crochet, D. Thomson, T. Carlson, 1987: MESO-GERS 84 Experiment: (A report to appear in *Bound.-Layer Meteor.*)

Wessels, H.R.A., 1984: Cabauw meteorological data tapes 1973-1984; description of instrumentation and data processing for the continuous measurements. KNMI

Scientific Report, WR-84-6. De Bilt, The Netherlands.

Wilczak, J.M. and J.A. Businger, 1984: Large-scale eddies in the unstably stratified atmospheric surface layer. Part II: Turbulent pressure fluctuations and the budgets of heat flux, stress, and turbulent kinetic energy. J. *Atmos. Sci.*, **41**, 3551-3567.

Willis, G.E. and J.W. Deardorff, 1974: A laboratory model of the unstable planetary boundary layer. *J. Atmos. Sci.*, **31**, 1297-1307.

Wyngaard, J.C. and O.R. Coté, 1971: The budgets of turbulent kinetic energy and temperature variance in the atmospheric surface layer. *J. Atmos. Sci.*, **28**, 190-201.